

Correlation-enhanced interaction of a Bose–Einstein condensate with parametric magnon pairs and virtual magnons

Victor S. L’vov,^{1,2,*} Anna Pomyalov,^{2,†} Dmytro A. Bozhko,^{3,‡} Burkard Hillebrands,^{4,§} and Alexander A. Serga^{4,¶}

¹*Department of Complex Systems, Weizmann Institute of Science, Rehovot 76100, Israel*

²*Department of Chemical and Biological Physics,
Weizmann Institute of Science, Rehovot 76100, Israel*

³*Department of Physics and Energy Science, University of Colorado Colorado Springs, Colorado Springs, Colorado 80918, USA*

⁴*Fachbereich Physik and Landesforschungszentrum OPTIMAS,
Rheinland-Pfälzische Technische Universität Kaiserslautern-Landau, 67663 Kaiserslautern, Germany*

Nonlinear interactions are crucial in science and engineering. Here, we investigate wave interactions in a highly nonlinear magnetic system driven by parametric pumping leading to Bose–Einstein condensation of spin-wave quanta—magnons. Using Brillouin light scattering spectroscopy in yttrium-iron garnet films, we found and identified a set of nonlinear processes resulting in off-resonant spin-wave excitations—virtual magnons. In particular, we discovered a dynamically-strong, correlation-enhanced four-wave interaction process of the magnon condensate with pairs of parametric magnons having opposite wavevectors and fully correlated phases.

Nonlinear wave interactions govern the behavior of various systems in nature, including processes in the Earth’s ocean and atmosphere [1], in stars [2], and even the evolution of the Universe [3]. In the field of magnetism, the use of nonlinear phenomena opens promising prospects for applications of magnonics and spintronics in neuromorphic computing, microwave data processing, and nanoscale wave logic circuits [4–8]. Spin waves, or magnons, in magnetically ordered materials are highly nonlinear compared to, for example, phonons or photons in solids. One of the best systems for studies of nonlinear spin-wave phenomena is the single-crystal ferrimagnetic yttrium iron garnet (YIG, $\text{Y}_3\text{Fe}_5\text{O}_{12}$) material [9, 10]. A strong magnon nonlinearity, combined with a high quality factor of magnons in YIG, facilitates the creation, registration, and study of various interaction processes.

The phenomenon of Bose–Einstein condensation of magnons at the bottom of their frequency spectrum, observed in YIG films [11–17], also develops through the nonlinear scattering of magnons. In our experiments, this condensation was achieved by the parametric pumping of magnons with microwave radiation [11, 16–20].

Here, we reveal several nonlinear processes that involve not only “real” quasiparticles—the eigenmodes of the medium—but produce, as a final result, virtual quasiparticles—out-of-resonance waves—caused by various types of nonlinear interactions. The most nontrivial process involves a pair of parametrically excited magnons and a Bose–Einstein condensate (BEC). This process is enhanced by full-phase correlations in parametric magnon pairs with opposite wavevectors \mathbf{q} and $-\mathbf{q}$.

Previously, virtual quasiparticles (e.g., virtual magnons) appeared in the theory of nonlinear waves [21–23] only as mathematical abstractions, mediating interactions between “real” quasiparticles. At the same time, the experimental observation of virtual quasiparticles is crucial for the identification of possible physical processes in nonlinear wave systems. This is especially critical

when, for various reasons, the experimental methods do not allow one to observe the real quasiparticles involved in these processes.

In our studies, we used Brillouin light scattering (BLS) spectroscopy [24, 25] employing a triple-pass tandem Fabry–Pérot interferometer [26]. Its high sensitivity enables the detection of a tiny number of magnons even at thermal noise level, and the frequency resolution (as low as 50 MHz) is quite sufficient for experiments with magnons in the 3–15 GHz range, which was explored in our investigation. The 532 nm laser beam is focused into a 20 μm diameter probing spot in the parametrically pumped area of the YIG film. By setting the incidence angle $\Theta_{q_{\parallel}}$ of this beam [27], the wavevectors of magnons propagating in the YIG film plane along the line of its intersection with the beam incidence plane are selected. Since, in our case, the incident plane is oriented along the direction of the bias magnetic field \mathbf{H} , magnons propagating in the same direction with wavevectors $\mathbf{q}_{\parallel} \parallel \mathbf{H}$ are detected. The change in the incidence angle from 0 to the maximal value of 58° in our experiment corresponds to the change in the detectable wavevectors from 0 to $2 \cdot 10^5 \text{ cm}^{-1}$. The wavevector resolution in our experiments is on the order of $\pm 10^3 \text{ cm}^{-1}$ [28].

Microwave pumping at 13.2 GHz is applied to the in-plane magnetized 6.7 μm -thick YIG film using a microstrip resonator of 50 μm width. In order to achieve high magnon occupation numbers $n(\omega, \mathbf{q})$, the pumping is supplied in pulses of up to 20 W and duration of 1 μs . A sufficiently low repetition rate of 1 kHz maintains a thermal quasi-equilibrium from pulse to pulse.

Our experimental results for the BLS intensity spectra $I(\omega, q_{\parallel})$, proportional to $n(\omega, q_{\parallel})$, are shown in Fig. 1. The solid red line shows the calculated magnon frequency spectrum $\omega_{q_{\parallel}}$ which has two minima $\omega_{\text{bot}} \equiv \min_{q_{\parallel}} \{\omega_{q_{\parallel}}\} \approx 4 \cdot (2\pi) \text{ GHz}$ at $q_{\parallel} = \pm q_{\text{bot}}$ with $q_{\text{bot}} \approx 4 \cdot 10^3 \text{ cm}^{-1}$. The two brightest spots in the vicinity of the bottom of the magnon spectra at $\pm q_{\text{bot}}$ originate from

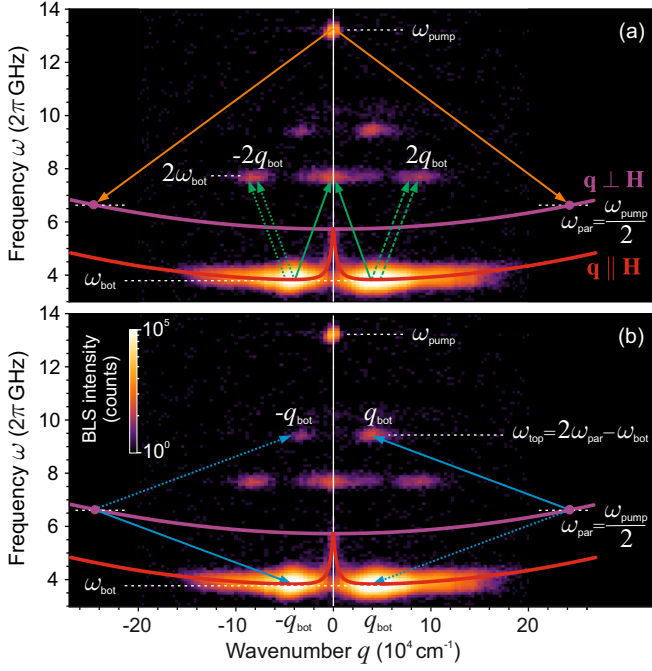


FIG. 1. Frequency- and wavevector-resolved BLS intensity spectra of real and virtual magnons. The spectra were measured during the action of microwave pumping in a YIG film magnetized in-plane by the field $H = 1350$ Oe. The experimental intensity spectra are shown together with the calculated magnon dispersion curves and diagrams representing the relevant quasiparticle scattering processes in the system. (a) The process of parametric pumping is shown by orange arrows. The signal of virtual “pump” magnons is visible at the pumping frequency ω_{pump} . The parametrically excited real magnons, marked by magenta dots, are outside the observation region. Virtual “double-bottom” magnons at the frequency $2\omega_{\text{bot}}$ arise due to the confluence of bottom magnons at ω_{bot} . The three types of confluence processes are indicated by pairs of green arrows. b) Processes of four-wave interaction of bottom magnons with phase-correlated pairs of parametric magnons leading to the appearance of virtual “top” magnons at the frequency ω_{top} are pairwise shown by the solid and dotted blue arrows [29].

“bottom” magnons associated with the left and right BEC states.

Above these brightest spots we see three spots with $\omega \approx 2\omega_{\text{bot}}$ and $q_{\text{left}} \approx -2q_{\text{bot}}$, $q_{\text{center}} \approx 0$, and $q_{\text{right}} \approx 2q_{\text{bot}}$. It is natural to relate them to the confluence of two bottom magnons, as shown by green arrows in Fig. 1(a):

- i) left spot, $\omega_{-q_{\parallel}} + \omega_{-q_{\parallel}} \Rightarrow 2\omega_{\text{bot}}$ and $q = -2q_{\text{bot}}$;
- ii) central spot, $\omega_{-q_{\parallel}} + \omega_{+q_{\parallel}} \Rightarrow 2\omega_{\text{bot}}$ and $q = 0$;
- iii) right spot, $\omega_{+q_{\parallel}} + \omega_{+q_{\parallel}} \Rightarrow 2\omega_{\text{bot}}$ and $q = 2q_{\text{bot}}$.

However, in our magnetization geometry, neither $\omega = 2\omega_{\text{bot}}$ with $q = \pm 2q_{\text{bot}}$ nor $\omega = 2\omega_{\text{bot}}$ with $q = 0$ are eigenmodes of the YIG film chosen. The only plausible explanation builds on the fact that we observe off-resonant waves driven by appropriate nonlinearity, i.e., virtual magnons. For brevity, we will call them “double-

bottom virtual magnons” [30].

In Fig. 1(a) the BLS spectra $I(\omega, q_{\parallel})$ are supplemented by two down-pointing orange arrows showing the process of parametric pumping by an external quasi-homogeneous microwave field with wavevector $\mathbf{q}_{\text{pump}} \approx 0$ and frequency ω_{pump} . Precisely at this position, we see a rather bright spot, indicating the presence of precession with this wavevector and frequency. Since there is no corresponding magnon eigenmode with $\omega = \omega_{\text{pump}}$, we observe here one more type of virtual magnon, called, for concreteness, virtual “pump” magnons. These magnons are directly driven by the external microwave magnetic field.

At the same time, we see no BLS response at the frequency of the parametrically pumped real magnons $\omega_{\text{par}} = \omega_{\text{pump}}/2$ because the wavenumbers of the parametric magnons are quite large and lie outside the sensitivity limit of our BLS setup at $\approx 2 \cdot 10^5 \text{ cm}^{-1}$. Nevertheless, these magnons are definitely present in the system [25], being responsible for the appearance of magnons at the bottom of the frequency spectrum [20, 31], which are clearly visible as extremely intense BLS signals.

In our previous studies [32–35], the magnon gas thermalization and BEC formation were developing in close interactions with the phonon bath [33, 36, 37], and leading to accumulation of hybrid magnon-phonon quasiparticles. In the present experiments, we observe no such phenomenon because the width of the pumping area is small, and the strong efflux of these quasiparticles leads to large losses for them [32].

Two more spots at $\omega_{\text{top}} = \omega_{\text{pump}} - \omega_{\text{bot}}$ and $q_{\text{top}} = \pm q_{\text{bot}}$, have a more sophisticated origin, which we discuss below within the classical Hamiltonian formalism convenient for description of nonlinear processes at large occupation numbers $n(\mathbf{q}) \gg 1$.

The classical Hamiltonian formalism is based on the equation of motion for the complex canonical wave amplitudes $a_{\mathbf{q}}$ and $a_{\mathbf{q}}^*$, which are classical limits of the Bose operators $\hat{a}_{\mathbf{q}}$ and $\hat{a}_{\mathbf{q}}^\dagger$ [21–23]:

$$\frac{da_{\mathbf{q}}(t)}{dt} = -i \frac{\delta \mathcal{H}}{\delta a_{\mathbf{q}}^*(t)}, \quad (1)$$

where \mathcal{H} is the Hamiltonian function, called for brevity the Hamiltonian.

For weakly interacting waves, \mathcal{H} can be expanded in $a_{\mathbf{q}}$ and $a_{\mathbf{q}}^*$ as $\mathcal{H} = \mathcal{H}_2 + \mathcal{H}_{\text{int}}$. The quadratic Hamiltonian $\mathcal{H}_2 = \sum_{\mathbf{q}} \omega_{\mathbf{q}} a_{\mathbf{q}} a_{\mathbf{q}}^*$ describes the free propagation of non-interacting waves with the dispersion law $\omega_{\mathbf{q}}$: $a_{\mathbf{q}}(t) \propto \exp[-i\omega_{\mathbf{q}}t]$. The interaction Hamiltonian $\mathcal{H}_{\text{int}} = \mathcal{H}_3 + \mathcal{H}_4$, includes

$$\mathcal{H}_3 = \frac{1}{2} \sum_{1,2,3} \left[V_{1,2}^3 a_1 a_2 a_3^* + (V_{1,2}^3)^* a_1^* a_2^* a_3 \right] \Delta_{1,2}^3, \quad (2a)$$

$$\mathcal{H}_4 = \frac{1}{4} \sum_{1,2,3,4} T_{1,2}^{3,4} a_1^* a_2^* a_3 a_4 \Delta_{1,2}^{3,4}. \quad (2b)$$

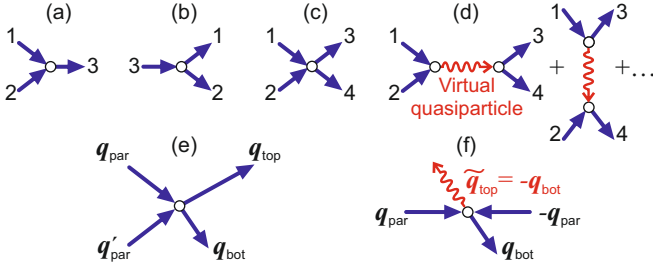


FIG. 2. Graphical representation of multi-wave scattering processes. Three-wave confluence (a) and splitting (b) processes given by Eq. (3). (c) The four-wave scattering process given by Eq. (4). (d) The first (see Eq. (7)) and second contribution to the 4-magnon scattering process in the second-order perturbation approach in the three-wave Hamiltonian, Eq. (2a). The red wavy lines show virtual quasiparticles, mediating these processes. All six contributions can be found, for example, in Eq.(1.1.32) from Ref. [22]. (e) Diagram of the four-magnon scattering [Eq. (8a)] leading to the kinetic instability of real magnons. (f) Diagram of the four-magnon scattering [Eq. (8a)] that leads to the excitation of the virtual “top” magnons.

Here, $V_{1,2}^3$ and $T_{1,2}^{3,4} = (T_{3,4}^{1,2})^*$ are three- and four-wave interaction amplitudes. The Kronecker symbols $\Delta_{1,2}^{3,4}$ and $\Delta_{1,2}^{3,4}$ are equal to one if the sum of “super-script” wavevectors equals the sum of “sub-script” wavevectors, and zero otherwise, taking care of wavevector conservation. For shortness, hereafter we use the notation $j \equiv \mathbf{q}_j$, with $j = 1, 2, 3, 4$.

The close analogy between the classical Hamiltonian and a quantum mechanical description allows for a physically transparent interpretation of the interactions \mathcal{H}_3 and \mathcal{H}_4 . Namely, \mathcal{H}_3 describes the process of the confluence of two waves (or two quasiparticles, such as magnons, phonons, etc.) with the wavevectors \mathbf{q}_1 and \mathbf{q}_2 into one wave with the wavevector $\mathbf{q}_3 = \mathbf{q}_1 + \mathbf{q}_2$, $2 \Rightarrow 1$ [see Fig. 2(a)], and the inverse process of decay of the \mathbf{q}_3 -wave into a pair of \mathbf{q}_1 - and \mathbf{q}_2 -waves, $1 \Rightarrow 2$ [see Fig. 2(b)]:

$$\omega_1 + \omega_2 \Leftrightarrow \omega_3. \quad (3)$$

Hamiltonian \mathcal{H}_4 is responsible for the $2 \Leftrightarrow 2$ scattering [see Fig. 2(c)] with the conservation laws

$$\omega_1 + \omega_2 \Leftrightarrow \omega_3 + \omega_4, \quad \mathbf{q}_1 + \mathbf{q}_2 = \mathbf{q}_3 + \mathbf{q}_4. \quad (4)$$

As a general rule, the $2 \Leftrightarrow 1$ processes are more efficient. When they are forbidden by the conservation law (3), one has to account for weaker scattering processes $2 \Leftrightarrow 2$, Eq. (4). Nevertheless, three-wave processes cannot be ignored in this case either. To see this, we examine equation Eq. (1) with the Hamiltonian (2):

$$\begin{aligned} \left[\frac{d}{dt} + i\omega_{\mathbf{q}} \right] a_{\mathbf{q}} = & -\frac{i}{2} \sum_{1,2} V_{1,2}^{\mathbf{q}} \Delta_{1,2}^{\mathbf{q}} a_1 a_2 \\ & + \sum_{1,2} (V_{\mathbf{q},2}^1)^* \Delta_{\mathbf{q},2}^1 a_1^* a_{\mathbf{q}} - \frac{i}{2} \sum_{2,3,4} T_{\mathbf{q},2}^{3,4} a_2^* a_3 a_4 \Delta_{\mathbf{q},2}^{3,4}. \end{aligned} \quad (5)$$

The first term in the right-hand side of Eq. (5) is the sum of off-resonant forces $F_{\mathbf{v}}(\mathbf{r}, t) \propto \exp\{i[\mathbf{q}_{\mathbf{v}} \cdot \mathbf{r}] - \omega_{\mathbf{v}} t\}$ with the wavevector $\mathbf{q}_{\mathbf{v}} = \mathbf{q}_1 + \mathbf{q}_2$ and frequency $\omega_{\mathbf{v}} = \omega_1 + \omega_2$. This force off-resonantly stirs up the driven wave

$$a(\mathbf{q}_1 + \mathbf{q}_2) = \sum_{1,2} V_{1,2}^{1+2} a_1 a_2 [2(\omega_1 + \omega_2 - \omega_{1+2})]^{-1}. \quad (6)$$

Taking a_1 and a_2 as $a_{\pm q_{\parallel}}$, we find the amplitudes of the virtual double magnons discussed above. By substituting $a(\mathbf{q}_1 + \mathbf{q}_2)$ from Eq. (6) into Eq. (2a) for the Hamiltonian \mathcal{H}_3 we find an additional contribution to the four-wave interaction amplitude

$$\delta T_{1,2}^{3,4} = V_{1,2}^{1+2} V_{1+2}^{3,4*} (\omega_1 + \omega_2 - \omega_{1+2})^{-1}, \quad (7)$$

arising in the second order of the perturbation theory by the amplitude of three-wave processes $V_{1,2}^3$ through the virtual wave with the frequency $\omega_{\mathbf{v}} = \omega_{1+2}$: $\omega_1 + \omega_2 \Rightarrow \omega_{1+2} \Rightarrow \omega_3 + \omega_4$. This process is shown in Fig. 2(d).

One can say that the process of nonlinear interaction of \mathbf{q}_1 - and \mathbf{q}_2 -quasiparticles generates the driving force $F_{\mathbf{v}}(\omega, \mathbf{q})$ with the frequency $\omega_{\mathbf{v}}$ and the wavevector $\mathbf{q}_{\mathbf{v}} = \mathbf{q}_1 + \mathbf{q}_2$. This force non-resonantly excites a wave perturbation in a nonlinear medium—a virtual quasiparticle with an amplitude $a_{q_{\mathbf{v}}}$ given by Eq. (6). The virtual quasiparticle decays into two real \mathbf{q}_3 - and \mathbf{q}_4 -quasiparticles with frequencies ω_3 and ω_4 resulting in a four-wave scattering process, Eqs. (4).

Returning to the analysis of our experimental results, note that in our geometry and for $H = 1350$ Oe the high population of the bottom magnons is the result of the so-called kinetic instability [20, 38, 39]: a four-magnon process (4) of decay of parametric magnons with frequency $\omega_1 = \omega_2 = \omega_{\text{par}} = \omega_{\text{pump}}/2$ and wavevectors $\mathbf{q}_1 = \mathbf{q}_{\text{par}}$, and $\mathbf{q}_2 = \mathbf{q}'_{\text{par}}$ into a pair of the bottom and the so-called “top” magnons with frequencies ω_{bot} and ω_{top} [see Fig. 2(e)]. If so, one expects

$$\omega_1 + \omega_2 = \omega_{\text{bot}} + \omega_{\text{top}} = \omega_{\text{pump}}, \quad \text{and} \quad (8a)$$

$$\mathbf{q}_1 + \mathbf{q}_2 = \pm \mathbf{q}_0 + \mathbf{q}_{\text{top}}. \quad (8b)$$

Assuming a rough estimate that $\omega_{\text{top}} \gg \omega_{\text{bot}}$, we conclude that $q_{\text{top}} > q_{\text{par}}$ meaning that the top magnons lie outside the sensitivity region of our BLS setup, i.e., they are invisible in Fig. 1. This raises the crucial question: What is the origin of the two spots in Fig. 1b at the “correct” frequency $\omega_{\text{top}} = \omega_{\text{pump}} - \omega_{\text{bot}}$, which is consistent with Eq. (8a), but with the experimentally observed wavevectors $\mathbf{q}_{\text{top}} = \pm \mathbf{q}_{\text{bot}}$, which completely disagree with Eq. (8b)?

To resolve this controversy, we note that the theory of kinetic instability is formulated in the framework of the weak-wave kinetic equation, which assumes weak correlations of the wave phases. As a result, the scattering (4) of real magnons has a stochastic nature and appears only as a second-order perturbation of the

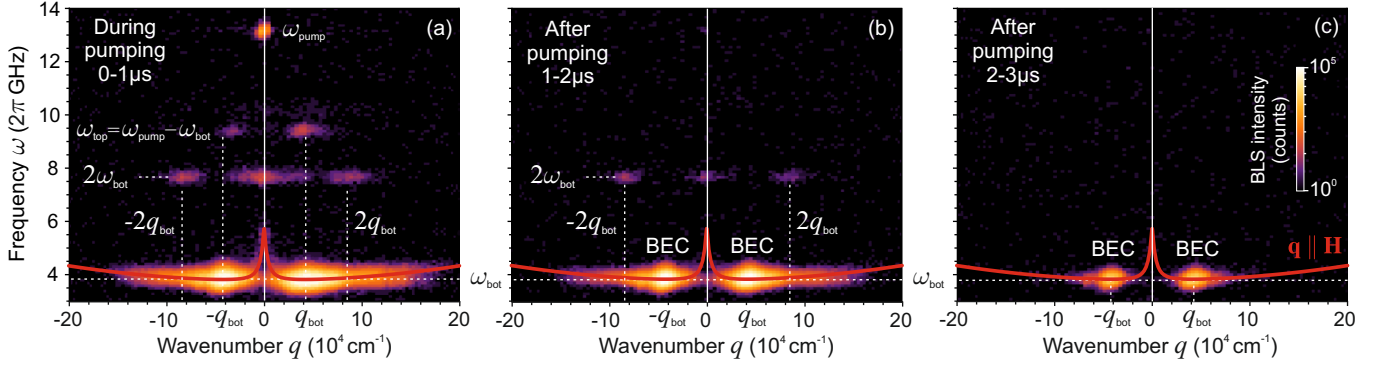


FIG. 3. Time evolution of the BLS spectra of the real and virtual magnons. (a) During the pumping microwave pulse, the virtual “top” magnons at $\omega_{\text{top}} = \omega_{\text{pump}} - \omega_{\text{bot}}$ are visible alongside with “double-bottom” virtual magnons at $2\omega_{\text{bot}}$. (b) Immediately after the pumping pulse, the virtual “top” magnons disappear, and only “double-bottom” virtual magnons are visible as the populations of magnon BECs at ω_{bot} are still large. (c) $2\mu\text{s}$ after the pumping pulse, only magnon BECs are visible. Due to the small magnon quantity, virtual magnons are not observable. All panels: the red solid curves show the calculated dispersion curves of magnons with uniform distributions of dynamic magnetization over the thickness of the YIG film and propagating in the film plane along the magnetization field \mathbf{H} .

four-wave interaction amplitudes $T_{1,2}^{3,4}$, Eq. (2b). Nevertheless, in our particular case with a large population of parametric and bottom magnons, the scattering waves have strong externally determined phase correlations. In particular, the full phase correlation in the pairs of parametric waves with $\pm \mathbf{q}_{\text{par}}$ arises due to their interaction with the space-homogeneous pumping field [22], thus $|\langle a_{\mathbf{q}_{\text{par}}} a_{-\mathbf{q}_{\text{par}}} \exp[i\omega_{\text{par}}] \rangle| = \langle |a_{\mathbf{q}_{\text{par}}}|^2 \rangle \equiv n_{\mathbf{q}_{\text{par}}}$. This allows us to consider a pair of parametric magnons ($a_{\mathbf{q}_{\text{par}}} a_{-\mathbf{q}_{\text{par}}}$) as a “single” wave object with the frequency $2\omega_{\text{par}} = \omega_{\text{pump}}$ and phase being the sum of the phases of the waves composing the pair. Therefore, due to its dynamic nature, the four-wave scattering process (4) with $\mathbf{q}_1 = -\mathbf{q}_2$, $\mathbf{q}_3 = \pm \mathbf{q}_{\text{bot}}$ is much stronger than stochastic scattering (4) with $\mathbf{q}_1 \neq -\mathbf{q}_2$, being now proportional to the first power of the interaction amplitude $T_{1,2}^{3,4}$. One can see this from the last term in the right-hand side of Eq. (5), which describes a driving force

$$\tilde{F}_V(\omega, \mp \mathbf{q}_{\text{bot}}) = \sum_{\mathbf{q}_{\text{par}}} T_{\mp \mathbf{q}_{\text{bot}}, \pm \mathbf{q}_{\text{bot}}}^{\mathbf{q}_{\text{par}}, -\mathbf{q}_{\text{par}}} a_2^* a_{\mathbf{q}_{\text{par}}} a_{-\mathbf{q}_{\text{par}}} \quad (9)$$

having the same frequency $\omega_{\text{top}} = \omega_{\text{pump}} - \omega_{\text{bot}}$ as that of real top magnons [see Eq. (8a)] and wavevector $\mathbf{q}_{\text{top}} = \mp \mathbf{q}_{\text{bot}}$. This force should off-resonantly excite virtual magnons with amplitude \tilde{a}_{top} , given by

$$\tilde{a}_{\text{top}}(\omega_{\text{top}}, \pm \mathbf{q}_{\text{bot}}) = \tilde{F}_V(\omega, \mp \mathbf{q}_{\text{bot}}) / [2(\omega_{\text{bot}} - \omega_{\text{par}})]. \quad (10)$$

In Fig. 1(b) one can see two bright spots exactly at $\omega = \omega_{\text{top}}$ and $\mathbf{q}_{\text{top}} \pm \mathbf{q}_{\text{bot}}$. We associate these spots with the “top” virtual magnons described above.

It is worth noting that such an enhancement of the efficiency of nonlinear processes in the case of phase-correlated waves is not a specific feature of the magnon system. For example, it is known in quantum optics for

simpler cases when only a few waves are involved in the interaction process [40].

To further confirm the origin of virtual magnons, we studied the evolution of magnons after the pumping is turned off. Figure 3 shows the BLS spectra of the real and virtual magnons at different moments of time. Figure 3(a) shows spectra during the pumping process (same as presented in Fig. 1, for reference). Figure 3(b) refers to the time interval $t = (1 - 2)\mu\text{s}$ after the pumping power has been turned off and the rapidly relaxing parametric magnons have disappeared. Therefore, we do not see the pump and top virtual magnons, forced either directly by the pumping magnetic field or through the parametric magnons, as seen in Fig. 2(f). The signal of the top virtual magnons disappears in a time not exceeding 20 ns. This value correlates well with earlier measurements of the scattering time of a group of parametrically pumped magnons, which in the BEC experiments was close to 10 ns [18]. Nevertheless, the double-bottom virtual magnons are still there, forced only by the bottom real magnons. They disappear only later, see Fig. 3(c), when the number of the (real) bottom magnons becomes too small to force the double magnons above a measurable level. Thus, the time evolution of the virtual magnons confirms the mechanism of their excitation suggested in our paper.

Traditionally, nonlinear-wave interactions are investigated via observation of “real” quasiparticles—quanta of freely propagating waves, i.e., eigenmodes of the nonlinear medium. In our experiments with highly populated magnon gases in a ferromagnetic YIG film, we found several types of virtual magnons—quanta of off-resonant spin waves—driven by real magnons through the appropriate nonlinearity. We show that virtual quasiparticles (virtual magnons in our case) may be the end result

of a new type of nonlinear processes in systems with narrow intense packets of quasiparticles. In particular, we discovered a four-wave interaction involving pairs of parametric waves with opposite wavevectors and a magnon Bose-Einstein condensate. This process is strongly enhanced by phase correlation in parametric pairs and BECs. The considered interactions that lead to the appearance of virtual quasiparticles contribute to the behavior of nonlinear systems, and are useful for the identification of physical processes in them. Furthermore, the study of various types of virtual and real quasiparticles and their correlation-enhanced interactions in the classical and quantum limit is necessary, for example, for their application in new technologies of information transfer and data processing [41], including coherent quantum optics, see e.g. [40] and references therein.

This study was funded by the Deutsche Forschungsgemeinschaft (DFG, German Research Foundation) – TRR 173/2 – 268565370 Spin+X (Project B04). D.A.B. acknowledges support by grant ECCS-2138236 from the National Science Foundation of the United States. V.S.L. was in part supported by NSF-BSF grant # 2020765. We thank R. Verba, P. Pirro and M. Fleischhauer, for fruitful discussions.

* victor.lvov@gmail.com

† anna.pomyalov@weizmann.ac.il

‡ dbozhko@uccs.edu

§ hilleb@physik.uni-kl.de

¶ serga@physik.uni-kl.de

- [1] S. Bartusek, K. Kornhuber, and M. Ting, 2021 North American heatwave amplified by climate change-driven nonlinear interactions, *Nat. Clim. Change* **12**, 1143 (2022).
- [2] C. Federrath, The turbulent formation of stars, *Phys. Today* **71**, 38 (2018).
- [3] M. Martinelli, I. Tutusaus, M. Archidiacono, S. Camera, V. F. Cardone, S. Clesse, S. Casas, L. Casarini, D. F. Mota, H. Hoekstra, C. Carbone, S. Ilić, T. D. Kitching, V. Pettorino, A. Pourtsidou, Z. Sakr, D. Sapone, N. Auricchio, A. Balestra, A. Boucaud, E. Branchini, M. Brescia, V. Capobianco, J. Carretero, M. Castellano, S. Cavuoti, A. Cimatti, R. Cledassou, G. Congedo, C. Conselice, L. Conversi, L. Corcione, A. Costille, M. Douspis, F. Dubath, S. Dusini, G. Fabbian, P. Fosalba, M. Frailis, E. Franceschi, B. Gillis, C. Giocoli, F. Grupp, L. Guzzo, W. Holmes, F. Hormuth, K. Jahnke, S. Kermiche, A. Kiessling, M. Kilbinger, M. Kunz, H. Kurki-Suonio, S. Ligorì, P. B. Lilje, I. Lloro, E. Maiorano, O. Marggraf, K. Markovic, R. Massey, M. Meneghetti, G. Meylan, B. Morin, L. Moscardini, S. Niemi, C. Padilla, S. Paltani, F. Pasian, K. Pedersen, S. Pires, G. Polenta, M. Poncet, L. Popa, F. Raison, J. Rhodes, M. Roncarelli, E. Rossetti, R. Saglia, P. Schneider, A. Secroun, S. Serrano, C. Sirignano, G. Sirri, J.-L. Starck, F. Sureau, A. N. Taylor, I. Tereno, R. Toledo-Moreo, E. A. Valentijn, L. Valenziano, T. Vassallo, Y. Wang, N. Welikala, A. Zacchei, and J. Zoubian, *Eur. Phys. J. Special Topics* **230**, 1005 (2021).
- [4] C. Koerner, R. Dreyer, M. Wagener, N. Liebing, H. G. Bauer, and G. Woltersdorf, Frequency multiplication by collective nanoscale spin-wave dynamics, *Science* **375**, 1165 (2022).
- [5] D. Turenne, A. Yaroslavtsev, X. Wang, V. Unikandani, I. Vaskivskiy, M. Schneider, E. Jal, R. Carley, G. Mercurio, R. Gort, N. Agarwal, B. V. Kuiken, L. Mercadier, J. Schlappa, L. L. Guyader, N. Gerasimova, M. Teichmann, D. Lomidze, A. Castoldi, D. Potorochin, D. Muktukavil, J. Brock, N. Z. Hagström, A. H. Reid, X. Shen, X. J. Wang, P. Maldonado, Y. Kvashnin, K. Carva, J. Wang, Y. K. Takahashi, E. E. Fullerton, S. Eisebitt, P. M. Oppeneer, S. Molodtsov, A. Scherz, S. Bonetti, E. Iacocca, and H. A. Dürr, Nonequilibrium sub-10 nm spin-wave soliton formation in FePt nanoparticles, *Sci. Adv.* **8**, eabn0523 (2022).
- [6] J. C. Gartside, K. D. Stenning, A. Vanstone, H. H. Holder, D. M. Arroo, T. Dion, F. Caravelli, H. Kurebayashi, and W. R. Branford, Reconfigurable training and reservoir computing in an artificial spin-vortex ice via spin-wave fingerprinting, *Nat. Nanotechnol.* **17**, 460 (2022).
- [7] Q. Wang, M. Kewenig, M. Schneider, R. Verba, F. Kohl, B. Heinz, M. Geilen, M. Mohseni, B. Lägél, F. Ciubotaru, C. Adelman, C. Dubs, S. D. Cotozana, O. V. Dobrovolskiy, T. Brächer, P. Pirro, and A. V. Chumak, A magnonic directional coupler for integrated magnonic half-adders, *Nat. Electron.* **3**, 765 (2020).
- [8] O. V. Prokopenko, D. A. Bozhko, V. S. Tyberkevych, A. V. Chumak, V. I. Vasyuchka, A. A. Serga, O. Dzyapko, R. V. Verba, A. V. Talalaevskij, D. V. Slobodianiuk, Y. V. Kobljanskyj, V. A. Moiseienko, S. V. Sholom, and V. Y. Malyshev, Recent trends in microwave magnetism and superconductivity, *Ukr. J. Phys.* **64**, 888 (2019).
- [9] V. Cherepanov, I. Kolokolov, and V. S. L'vov, The saga of YIG: Spectra, thermodynamics, interaction and relaxation of magnons in a complex magnet, *Phys. Rep.* **229**, 81 (1993).
- [10] A. Z. Arsal, A. W. M. Zuhdi, N. B. Ibrahim, and M. A. Hannan, Recent advances in yttrium iron garnet films: Methodologies, characterization, properties, applications, and bibliometric analysis for future research directions, *Appl. Sci.* **13**, 1218 (2023).
- [11] S. O. Demokritov, V. E. Demidov, O. Dzyapko, G. A. Melkov, A. A. Serga, B. Hillebrands, and A. N. Slavin, Bose-Einstein condensation of quasi-equilibrium magnons at room temperature under pumping, *Nature* **443**, 430 (2006).
- [12] C. Safranski, I. Barsukov, H. K. Lee, T. Schneider, A. A. Jara, A. Smith, H. Chang, K. Lenz, J. Lindner, Y. Tserkovnyak, M. Wu, and I. N. Krivorotov, Spin caloritronic nano-oscillator, *Nat. Commun.* **8**, 117 (2017).
- [13] M. Schneider, T. Brächer, D. Breitbach, V. Lauer, P. Pirro, D. A. Bozhko, H. Y. Musienko-Shmarova, B. Heinz, Q. Wang, T. Meyer, F. Heussner, S. Keller, E. T. Papaioannou, B. Lägél, T. Löber, C. Dubs, A. N. Slavin, V. S. Tiberkevich, A. A. Serga, B. Hillebrands, and A. V. Chumak, Bose-Einstein condensation of quasi-

- particles by rapid cooling, *Nat. Nanotechnol.* **15**, 457 (2020).
- [14] M. Schneider, D. Breitbach, R. O. Serha, Q. Wang, A. A. Serga, A. N. Slavin, V. S. Tiberkevich, B. Heinz, B. Lagel, T. Bracher, C. Dubs, S. Knauer, O. V. Dobrovolskiy, P. Pirro, B. Hillebrands, and A. V. Chumak, Control of the Bose–Einstein condensation of magnons by the spin Hall effect, *Phys. Rev. Lett.* **127**, 237203 (2021).
- [15] B. Divinskiy, H. Merbouche, V. E. Demidov, K. O. Nikolaev, L. Soumah, D. Gouere, R. Lebrun, V. Cros, J. B. Youssef, P. Bortolotti, A. Anane, and S. O. Demokritov, Evidence for spin current driven Bose–Einstein condensation of magnons, *Nat. Commun.* **12**, 6541 (2021).
- [16] O. Dzyapko, P. Nowik-Boltyk, B. Koene, V. E. Demidov, J. Jersch, A. Kirilyuk, T. Rasing, and S. O. Demokritov, High-resolution magneto-optical Kerr-effect spectroscopy of magnon Bose–Einstein condensate, *IEEE Magn. Lett.* **7**, 1 (2016).
- [17] T. B. Noack, V. I. Vasyuchka, A. Pomyalov, V. S. L’vov, A. A. Serga, and B. Hillebrands, Evolution of room-temperature magnon gas: Toward a coherent Bose–Einstein condensate, *Phys. Rev. B* **104**, L100410 (2021).
- [18] A. A. Serga, V. S. Tiberkevich, C. W. Sandweg, V. I. Vasyuchka, D. A. Bozhko, A. V. Chumak, T. Neumann, B. Obry, G. A. Melkov, A. N. Slavin, and B. Hillebrands, Bose–Einstein condensation in an ultra-hot gas of pumped magnons, *Nat. Commun.* **5**, 3452 (2014).
- [19] P. Clausen, D. A. Bozhko, V. I. Vasyuchka, B. Hillebrands, G. A. Melkov, and A. A. Serga, Stimulated thermalization of a parametrically driven magnon gas as a prerequisite for Bose–Einstein magnon condensation, *Phys. Rev. B* **91**, 220402 (2015).
- [20] A. J. Kreil, D. A. Bozhko, H. Y. Musiienko-Shmarova, V. I. Vasyuchka, V. S. L’vov, A. Pomyalov, B. Hillebrands, and A. A. Serga, From kinetic instability to Bose–Einstein condensation and magnon supercurrents, *Phys. Rev. Lett.* **121**, 077203 (2018).
- [21] V. E. Zakharov, V. S. L’vov, and G. Falkovich, *Kolmogorov Spectra of Turbulence I. Wave Turbulence*, Springer Series in Nonlinear Dynamics (Springer-Verlag, 1992).
- [22] V. S. L’vov, *Wave Turbulence Under Parametric Excitation. Applications to Magnets*, Springer Series in Nonlinear Dynamics (Springer-Verlag, 1994).
- [23] S. Nazarenko, *Wave Turbulence*, Lecture Notes in Physics, Vol. 825 (Springer-Verlag, 2011).
- [24] B. Hillebrands, Brillouin light scattering from layered magnetic structures, in *Light Scattering in Solids VII: Crystal-Field and Magnetic Excitations*, edited by M. Cardona and G. Guntherodt (Springer, 2000) pp. 174–289.
- [25] A. A. Serga, C. W. Sandweg, V. I. Vasyuchka, M. B. Jungfleisch, B. Hillebrands, A. Kreisel, P. Kopietz, and M. P. Kostylev, Brillouin light scattering spectroscopy of parametrically excited dipole-exchange magnons, *Phys. Rev. B* **86**, 134403 (2012).
- [26] R. Mock, B. Hillebrands, and R. Sandercock, Construction and performance of a Brillouin scattering set-up using a triple-pass tandem Fabry–Perot interferometer, *J. Phys. E.* **20**, 656 (1987).
- [27] D. A. Bozhko, H. Y. Musiienko-Shmarova, V. S. Tiberkevich, A. N. Slavin, I. I. Syvorotka, B. Hillebrands, and A. A. Serga, Unconventional spin currents in magnetic films, *Phys. Rev. Res.* **2**, 023324 (2020).
- [28] C. W. Sandweg, M. B. Jungfleisch, V. I. Vasyuchka, A. A. Serga, P. Clausen, H. Schultheiss, B. Hillebrands, A. Kreisel, and P. Kopietz, Wide-range wavevector selectivity of magnon gases in Brillouin light scattering spectroscopy, *Rev. Sci. Instrum.* **81**, 073902 (2010).
- [29] To the same result leads the scattering process in which the parametric magnon q_{par} scatters to the virtual state $(\omega_{\text{top}}, -q_{\text{bot}})$, and the magnon $-q_{\text{par}}$ to the state $(\omega_{\text{bot}}, q_{\text{bot}})$, and also symmetric to it, when the parametric magnon q_{par} scatters to the state $(\omega_{\text{bot}}, -q_{\text{bot}})$, and the magnon $-q_{\text{par}}$ to the virtual state $(\omega_{\text{top}}, q_{\text{bot}})$.
- [30] The BLS spectral peaks caused by off-resonant confluence processes can also be seen in Fig. 3 in M. Geilen, R. Verba, A. Nicoloiu, D. Narducci, A. Dinescu, M. Ender, M. Mohseni, F. Ciubotaru, M. Weiler, A. Muller, B. Hillebrands, C. Adelman, and P. Pirro, Parametric excitation and instabilities of spin waves driven by surface acoustic waves, (2022), arXiv:2201.04033.
- [31] D. A. Bozhko, P. Clausen, A. V. Chumak, Y. V. Kobljanskyj, B. Hillebrands, and A. A. Serga, Formation of Bose–Einstein magnon condensate via dipolar and exchange thermalization channels, *Low Temp. Phys.* **41**, 801 (2015).
- [32] D. A. Bozhko, P. Clausen, G. A. Melkov, V. S. L’vov, A. Pomyalov, V. I. Vasyuchka, A. V. Chumak, B. Hillebrands, and A. A. Serga, Bottleneck accumulation of hybrid magnetoelastic bosons, *Phys. Rev. Lett.* **118**, 237201 (2017).
- [33] D. A. Bozhko, V. I. Vasyuchka, A. V. Chumak, and A. A. Serga, Magnon-phonon interactions in magnon spintronics (Review article), *Low Temp. Phys.* **46**, 383 (2020).
- [34] P. Frey, D. A. Bozhko, V. S. L’vov, B. Hillebrands, and A. A. Serga, Double accumulation and anisotropic transport of magnetoelastic bosons in yttrium iron garnet films, *Phys. Rev. B* **104**, 014420 (2021).
- [35] V. Hahn, P. Frey, A. A. Serga, V. I. Vasyuchka, B. Hillebrands, P. Kopietz, and A. Ruckriegel, Accumulation of magnetoelastic bosons in yttrium iron garnet: Kinetic theory and wave-vector-resolved Brillouin light scattering, *Phys. Rev. B* **105**, 144421 (2022).
- [36] J. Hick, F. Sauli, A. Kreisel, and P. Kopietz, Bose–Einstein condensation at finite momentum and magnon condensation in thin film ferromagnets, *Eur. Phys. J. B* **78**, 429 (2010).
- [37] A. Ruckriegel, P. Kopietz, D. A. Bozhko, A. A. Serga, and B. Hillebrands, Magnetoelastic modes and lifetime of magnons in thin yttrium iron garnet films, *Phys. Rev. B* **89**, 184413 (2014).
- [38] A. V. Lavrinenko, V. S. L’vov, G. A. Melkov, and V. B. Cherepanov, “Kinetic” instability of a strongly nonequilibrium system of spin waves and tunable radiation of a ferrite, *Sov. Phys. JETP* **54**, 542 (1981).
- [39] G. A. Melkov and S. V. Sholom, Kinetic instability of spin waves in thin ferrite films, *Sov. Phys. JETP* **72**, 341 (1991).
- [40] P. Turschmann, H. L. Jeannic, S. F. Simonsen, H. R. Haakha, S. Gotzinger, V. Sandoghdar, P. Lodahl, and R. Nir, Coherent nonlinear optics of quantum emitters in nanophotonic waveguides, *Nanophotonics* **10**, 1641–1657 (2019).
- [41] M. Fukami, D. R. Candido, D. D. Awschalom, and M. E. Flatte, Opportunities for long-range magnon-mediated entanglement of spin qubits via on- and off-resonant coupling, *PRX Quantum* **2**, 040314 (2021).